# Dalton Transactions

Accepted Manuscript

Journal Name

RSCPublishing

COMMUNICATION

# Mechanism of Hydrogen Evolution in Cu(bztpen)-Catalysed Water Reduction: A DFT Study

Cite this: DOI: 10.1039/x0xx00000x

Rong-Zhen Liao,[*a] Mei Wang,[b] Licheng Sun,[b,c] and Per E. M. Siegbahn[*d]

Received 00th January 2012,
Accepted 00th January 2012

DOI: 10.1039/x0xx00000x

www.rsc.org/

**The mechanism of water reduction catalysed by a mononuclear copper complex Cu(bztpen) (bztpen= *N*-benzyl-*N*,*N'*,*N'*-tris(pyridine-2-ylmethyl)ethylenediamine) has been elucidated by DFT calculations, revealing that hydrogen evolution proceeds via coupling of a Cu(II)-hydride and a pendant pyridinium, and providing important implications for the future design of new catalytic systems for water reduction.**

The sustainable production of clean fuels, like molecular hydrogen, has emerged as one of the major scientific challenges of this century.[1] Extraordinary efforts have been dedicated into the design of water reduction electrocatalysts that embrace only earth-abundant transition metals and exhibit high turnover frequency (TOF) and turnover number (TON) with relatively low overpotentials. A variety of molecular electrocatalysts on the basis of iron,[2] cobalt,[3] nickel,[4] and molybdenum[5] have been reported for hydrogen evolution in aqueous solutions. Very recently, Wang and co-workers reported the first mononuclear copper complex $Cu^{II}$(bztpen) that has been shown to act as a very efficient electrocatalyst for $H_2$ production in a phosphate buffer at pH 2.5 with an onset overpotential of 0.42 V.[6]

The crystal structure of $[Cu^{II}(bztpen)](BF_4)_2$ shows a distorted trigonal-bipyramidal coordination mode, in which a pyridine group and an amine group are situated at the axial positions.[6] Differential pulse voltammetry (CV) measurement of the catalyst in phosphate buffer (pH = 2.5) showed a reversible peak at $E_{1/2} = -0.03$ V, which was assigned to be a $Cu^{II}/Cu^{I}$ redox process. This is followed by a water reduction catalytic peak at −0.82 V. Importantly, both reductions were found to be proton-coupled electron transfer (PCET) processes. With an applied potential of −0.60 V, the TOF was measured to be 1450 mol $H_2$ (mol cat)$^{-1}$ h$^{-1}$ cm$^{-2}$ ($k_{obs}$ larger than 10000 s$^{-1}$), with a TON of 2900 mol $H_2$ (mol cat)$^{-1}$ cm$^{-2}$ in two hours. Two different mechanistic scenarios (Scheme 1) have been proposed for the hydrogen evolution. They differ mainly by where the proton enters upon the first reduction of $Cu^{II}$ to $Cu^{I}$. If the proton goes to the metal, a $Cu^{III}$-hydride species is formed; or a $Cu^{I}$-pyridinium species is formed if the pyridine gets protonated. The latter pathway appears to be more likely on the basis of UV/Vis and $^1$H NMR spectroscopic studies.[6]

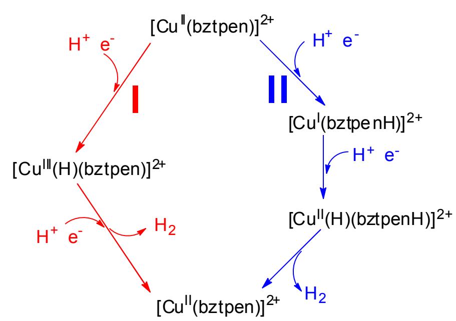


**Scheme 1** Two possible pathways for $H_2$ production catalysed by $[Cu^{II}(bztpen)]^{2+}$.

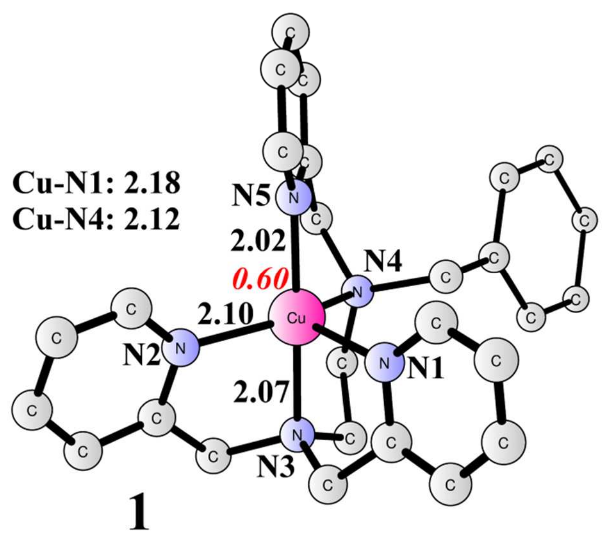


**Fig. 1** Optimized structure of $[Cu^{II}(bztpen)]^{2+}$ (**1**). Distances are given in Ångstrom. Spin density on Cu is shown in red italic.

Inspired by this intriguing catalyst, we performed density functional calculations[7] at the B3LYP*-D3/SDD-6-311+G(2df,2p)//B3LYP/SDD-6-31G(d,p) level[8] to investigate the detailed redox processes and the $H_2$ formation mechanism. Our findings will provide important implications for the future design of new catalytic systems for electrocatalytic water reduction.

Our investigation starts from $[Cu^{II}(bztpen)]^{2+}$ (labelled as **1**), and the optimized structure of which is shown in Fig. 1. Geometry optimization of **1** gave the Cu–N bonds in the range of 2.02–2.18 Å, which are in good agreement with the crystal structure (ranging from 1.99–2.13 Å).[6] In addition, overlay of the optimized structure and the crystal structure gave a RMSD of 0.16 Å (see Fig. S1 in ESI†). The spin state of **1** is a doublet and the spin density on Cu is 0.60 due to partial spin delocalization to the ligand. The p*K*a of the protonated form $\mathbf{1_{pt}}$ (structures of three isomers see Fig. S2 in ESI†) is -1.5, suggesting that **1** is the major species in solution at pH 2.5.

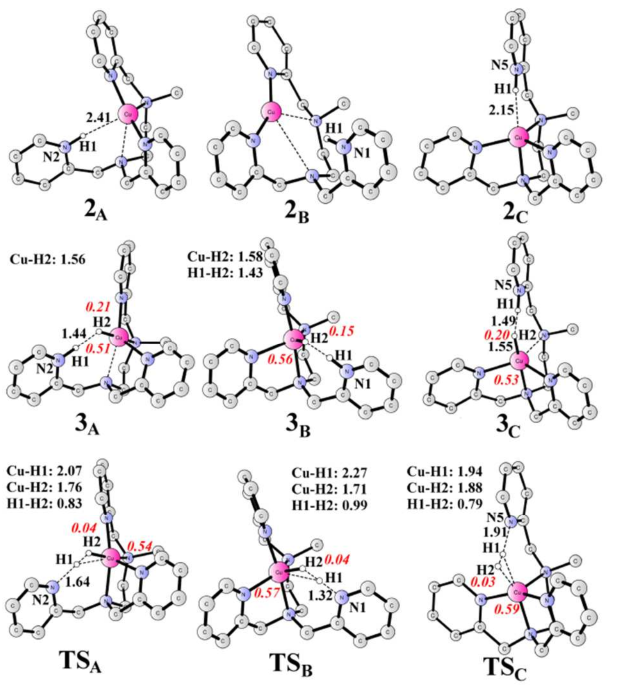


**Fig. 2** Optimized isomers of **2**, **3**, and the $H_2$ formation transition state (**TS**). Distances are given in Ångstrom. For clarity, unimportant hydrogen atoms and the phenyl ring are not shown. Spin densities on Cu and H2 in **3** and **TS** are shown in red italic.

At pH 2.5, the first reduction to generate a closed-shell singlet species **2** (Fig. 2) is a PCET process, in which the electron is added to reduce $Cu^{II}$ to $Cu^{I}$, in concomitant with the protonation of a pyridine group (p*K*a of **2** being 6.0, the structure of the deprotonated form is shown in Fig. S3 in ESI†). The reduction potential for the **2**/**1** couple was calculated to be −0.21 V, with a difference of 0.18 V compared with experimental one.[6] Three different isomers ($\mathbf{2_A}$, $\mathbf{2_B}$, and $\mathbf{2_C}$) can be located, depending on whether the proton goes to N2, N1, or N5. The isomer $\mathbf{2_A}$ was calculated to be the most stable one, and the energies of $\mathbf{2_B}$ and $\mathbf{2_C}$ are 0.1 and 5.3 kcal $mol^{-1}$ higher than that of $\mathbf{2_A}$, respectively. Interconversion between $\mathbf{2_A}$, $\mathbf{2_B}$, and $\mathbf{2_C}$ can easily take place, and the potential energy profile is shown in Fig. 3 (For the structures, see Fig. S4 in ESI†). From $\mathbf{2_A}$ to $\mathbf{2_B}$, the barrier is only 9.6 kcal $mol^{-1}$, while it is 14.3 kcal $mol^{-1}$ from $\mathbf{2_A}$ to $\mathbf{2_C}$. These results suggest that $\mathbf{2_A}$ and $\mathbf{2_B}$ are the dominant species and they are in a fast equilibrium. This agrees very well with the experimental $^{1}H$ NMR results, which suggest two equivalent pyridine moieties are in a fast association/dissociation equilibrium.[6] Protonation of $Cu^{I}$ to form a $Cu^{III}$-hydride intermediate (Figs. S5 and S6 in ESI†) was also considered. The energy of this step is as high as 41.3 kcal $mol^{-1}$ relative to the energy of $\mathbf{2_A}$. This is different from mononuclear Fe and Co-based catalysts, in which protonation of $M^{I}$ (M = Fe or Co) is feasible to generate $M^{III}$-hydride.[9] Since the generation of $Cu^{III}$-hydride is thermodynamically very unfeasible, we can safely rule out pathway **I** in Scheme 1 as a viable option.

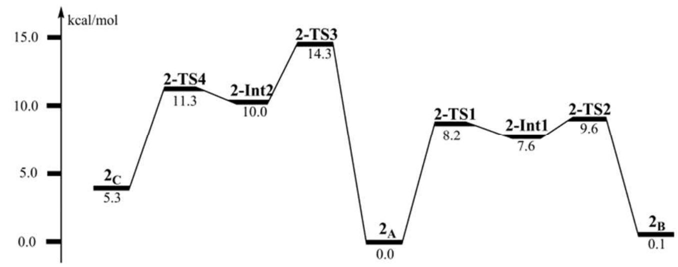


**Fig. 3** Gibbs free energy profile for the interconversion of $\mathbf{2_A}$, $\mathbf{2_B}$, and $\mathbf{2_C}$.

Two alternative pathways to generate **2** from **1** have also been considered, namely proton transfer followed by electron transfer (PTET) and electron transfer followed by proton transfer (ETPT). For the PTET pathway, the protonation of **1** at pH 2.5 is endergonic by 5.5 kcal/mol (Fig. 4), and the following reduction has a potential of 0.03 V. For the ETPT pathway, the one electron reduction to generate $\mathbf{2_{dp}}$ has a potential of -0.64 V. In $\mathbf{2_{dp}}$, the $Cu^{I}$ ion is penta-coordinated, and in order to make one of the pyridine ligands protonated, one pyridine ligand has to dissociate from the metal center to form $\mathbf{2_{dp'}}$ (structures of three isomers see Fig. S3). This process is endergonic by 3.1 kcal/mol (Fig. 4). When a potential of -0.6 V is applied, the formation of $\mathbf{2_{dp'}}$ from **1** is endergonic by 4.0 kcal/mol. These results are consistent with the experimental observation, which shows a PCET pathway.[6]

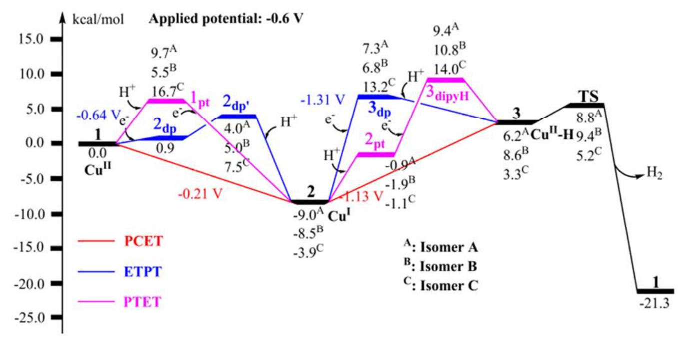


**Fig. 4** Gibbs free energy diagram for the water reduction catalysed by **1**.

The subsequent reduction is also a PCET step with a potential of −1.13 V (experiment: −0.82 V) to generate a $Cu^{II}$-hydride intermediate **3** (p*K*a = 5.1, the structures of the deprotonated forms are shown in Fig. S7 in ESI†), with a doublet spin state. Consistently, three isomers were optimized. Unexpectedly, $\mathbf{3_C}$ has the lowest energy, while $\mathbf{3_A}$ and $\mathbf{3_B}$ lie +2.9 and +5.3 kcal $mol^{-1}$ higher than **3c**, respectively. In $\mathbf{3_C}$, the Cu-H2 bond is 1.55 Å, the spin densities on Cu and H2 are 0.53 and 0.20, respectively. The distance between H1 and H2 is only 1.49 Å, suggesting the formation of a unconventional hydrogen bond,[10] and thus the hydride is ready for protonation to evolve $H_2$. It is also possible that the proton goes to a second pyridine group rather than the metal, thus generating a $Cu^{0}$ di-pyridinium intermediate ($\mathbf{3_{dipyH}}$, Fig. S8 in ESI†). However, the energy required to form the dipyridinium species is 6.1 kcal $mol^{-1}$ higher than to form the $Cu^{II}$-hydride, suggesting that the generation of a $Cu^{II}$-hydride is preferred. This is also important for the following H–H bond formation, as the coupling of a $Cu^{II}$-hydride and a pendant pyridinium should be facile.

Similarly to the **2/1** reduction, both ETPT and PTET pathways for the **3/2** reduction are thermodynamically less favourable (Fig. 4). For the ETPT pathway, the one electron reduction potential for $\mathbf{3_{dp}/2}$ is -1.31 V, suggesting that the formation of $\mathbf{3_{dp}}$ is endergonic by 15.8 kcal/mol with an applied potential of -0.6 V. For the PTET pathway, the p*K*a of $\mathbf{2_{pt}}$ (Fig. S9 in ESI†) is calculated to be -2.7, implying that its formation is endergonic by 7.1 kcal/mol at pH 2.5. The following one electron reduction from $\mathbf{2_{pt}}$ to form $\mathbf{3_{dipyH}}$ has a potential of -1.09 V. Therefore, the formation of $\mathbf{3_{dipyH}}$ from **2** is endergonic by 18.4 kcal/mol. From a theoretical point of view, it is possible that the ETPT and/or PTET pathways are kinetically favoured even though they are thermodynamically less favoured. To model and calculate the kinetics (transition state and rate) for such an electrochemical process, which involves electron transfer from the electrode to the catalyst, is very difficult. However, for the present case, the experimental results already suggested a PCET process for both the **2/1** and **3/2** reductions.[6]

The transition states (**TS**) for the H–H bond formation are optimized for each isomer and shown in Fig. 2. The $\mathbf{TS_C}$ has a barrier of only 1.9 kcal $mol^{-1}$ relative to $\mathbf{3_C}$. If a potential of −0.6 V is applied (Fig. 4), the barrier of $\mathbf{TS_C}$ is 14.2 kcal $mol^{-1}$ relative to $\mathbf{2_A}$, including an energetic penalty of 12.3 kcal $mol^{-1}$ required for converting $\mathbf{2_A}$ to $\mathbf{3_C}$. However, the barrier for the interconversion between $\mathbf{2_A}$ and $\mathbf{2_C}$ is 14.3 kcal $mol^{-1}$ (Fig. 3), which is almost the same as that for $H_2$ formation. Both transition states should thus contribute to the rate-limiting turnover of the catalyst. The $H_2$ formation via $\mathbf{TS_A}$ and $\mathbf{TS_B}$ is not preferred as their barriers are higher (17.8 and 18.4 kcal $mol^{-1}$, respectively). If a potential of −0.9 V is applied, the energy of $\mathbf{TS_C}$ becomes 7.3 kcal $mol^{-1}$ relative to $\mathbf{2_A}$. This is lower than the barrier for the conversion of $\mathbf{2_A}$ to $\mathbf{2_C}$, which is required for the following $H_2$ formation step via $\mathbf{TS_C}$. Consequently, the conversion of $\mathbf{2_A}$ to $\mathbf{2_C}$ becomes rate-limiting and the total barrier is 14.3 kcal $mol^{-1}$ for this pathway. However, the total barrier for $\mathbf{TS_A}$ in this case is only 10.9 kcal $mol^{-1}$, suggesting that there is no need of conversion of $\mathbf{2_A}$ to $\mathbf{2_C}$ and that $H_2$ formation proceeds via $\mathbf{TS_A}$ directly. The calculated barrier of 10.9 kcal $mol^{-1}$ is consistent with the very large $k_{obs}$ (larger than 10000 $s^{-1}$) determined by experiment,[6] which can be converted into barrier of about 10–11 kcal $mol^{-1}$ using the classical transition state theory. It should be pointed out that the reduction of **2** to **3** might contribute to the rate-limiting turnover when a very negative potential is applied as the formation of $H_2$ is very fast. The nature of $\mathbf{TS_C}$ was confirmed to have only one imaginary frequency of 193.6*i* $cm^{-1}$, which corresponds to the H1–H2 bond formation. At $\mathbf{TS_C}$, the critical H1–H2, N5–H1, and Cu–H2 distances are 0.79, 1.91, and 1.88 Å, respectively. Downhill from $\mathbf{TS_C}$, $H_2$ dissociates from Cu to regenerate **1** and no stable $Cu^{II}$-$H_2$ adduct can be located, which was confirmed by IRC[11] calculations (Fig. S10 in ESI†). In this mechanism, one of the three pyridine groups functions as a pendant base to take a proton during the first reduction, which reacts with the $Cu^{II}$-hydride created by the second reduction. This scenario also mimics the mechanism for the H–H bond formation/cleavage catalysed by [NiFe] and [FeFe]hydrogenase.[12] In addition, the critical role of a pendant base has been discussed by DFT calculations on a [FeFe]-hydrogenase model.[13]

In conclusion, we have investigated the mechanism for the $[Cu^{II}(bztpen)]$-catalysed water reduction. Both the two experimentally-proposed pathways were examined, and the one with the involvement of a $Cu^{III}$-hydride as a key intermediate was ruled out due to its very high energy. The reaction starts with a PCET to generate a $Cu^{I}$–pyridinium intermediate, in which the proton can transfer between two pyridine groups in a fast equilibrium. The following PCET leads to the formation of a $Cu^{II}$-hydride intermediate, which is followed by H–H bond formation by coupling the $Cu^{II}$-hydride and the pyridinium group. The pendant pyridine group plays an important role in lowering the barrier for $H_2$ formation. $H_2$ release takes place directly after H–H bond formation, without the formation of a stable $Cu^{II}$-$H_2$ adduct. The total barrier for the H–H bond formation was calculated to be 14.3 kcal $mol^{-1}$ with an applied potential of −0.6 V, and only 10.9 kcal $mol^{-1}$ with an applied potential of −0.9 V. These findings provide a basis for the future design of copper-based water reduction electrocatalysts with high efficiency and low overpotential.

This work was supported by startup funding from Huazhong University of Science and Technology, the Swedish Research Council, and the Knut and Alice Wallenberg Foundation. Computer time was generously provided by the Swedish National Infrastructure for Computing.

## Notes and references

[a] Key Laboratory for Large-Format Battery Materials and System, Ministry of Education, School of Chemistry and Chemical Engineering, Huazhong University of Science and Technology, Wuhan 430074, China. E-mail: rongzhen@hust.edu.cn

[b] State Key Laboratory of Fine Chemicals, DUT-KTH Joint Education and Research Center on Molecular Devices, Dalian University of Technology (DUT), Dalian 116024, China.

[c] Department of Chemistry, KTH Royal Institute of Technology, Stockholm 10044, Sweden.

[d] Department of Organic Chemistry, Arrhenius Laboratory, Stockholm University, SE-10691 Stockholm, Sweden. E-mail: ps@organ.su.se

† Electronic Supplementary Information (ESI) available: Computational details and Coordinates for all structures. See DOI: 10.1039/c000000x/

1 J. A. Turner *Science*, 2004, **305**, 972-974; T. R. Cook, D. K. Dogutan, S. Y. Reece, Y. Surendranath, T. S. Teets, D. G. Nocera, *Chem. Rev.*, 2010, **110**, 6474-6502.

2 (a) R. Mejia-Rodriguez, D. Chong, J. H. Reibenspies, M. P. Soriaga, M. Y. Darensbourg, *J. Am. Chem. Soc.,* 2004, **126**, 12004-12014. (b) Y. Na, M. Wang, K. Jin, R. Zhang, L. Sun, *J. Organomet. Chem.*, 2006, **691**, 5045-5051. (c) F. Quentel, G. Passard, F. Gloaguen, *Energy Environ. Sci.*,2012, **5**, 7757-7761.

3 (a) B. D. Stubbert, J. C. Peters, H. B. Gray, *J. Am. Chem. Soc.,* 2011, **133**, 18070-18073. (b) Y. Sun, J. Sun, J. R. Long, P. Yang, C. J. Chang, *Chem. Sci.*, 2013, **4**, 118-124. (c) P. Zhang, F. Gloaguen, F. Quentel, *Chem. Comm.*, 2013, **49**, 9455-9457. (d) L. Chen, M. Wang, K. Han, P. Zhang, F. Gloaguen, L. Sun, *Energy Environ. Sci.*,2014, 7, 329-334.

4 (a) O. R. Luca, S. J. Konezny, J. D. Blakemore, D. M. Colosi, S. Saha, G. W. Brudvig, V. S. Bastista, R. H. Crabtree, *New. J. Chem.*, 2012, **36**, 1149-1152. (b) P. Zhang, M. Wang, Y. Yang, D. Zheng, K. Han, L. Sun, *Chem. Comm.*, 2014, **50**, 14153-14156.

5 (a) H. I. Karunadasa, C. J. Chang, J. R. Long, *Nature*, 2010, **464**, 1329-1333.(b) H. I. Karunadasa, E. Montalvo, Y. Sun, M. Majda, J. R. Long, C. J. Chang, *Science*, 2012, **335**, 698-702.

6 P. Zhang, M. Wang, Y. Yang, T. Yao, L. Sun, *Angew. Chem. Int. Ed.*, 2014, **53**, 13803-13807.
7 For computational details, see the ESI†.
8 (a) A. D. Becke, *J. Chem. Phys.,* 1993, **98**, 5648-5652. (b) M. Reiher, O. Salomon, B. A. Hess, *Theor. Chem. Acc.,* 2001, **107**, 48-55.
9 (a) B. H. Solis, S. Hammes-Schiffer, *J. Am. Chem. Soc.*, 2011, **133**, 19036-19039. (b) B. H. Solis, S. Hammes-Schiffer, *Inorg. Chem*., 2011, **50**, 11252-11262. (c) B. H. Solis, S. Hammes-Schiffer, *J. Am. Chem. Soc.*, 2012, **134**, 15253-15256. (d) B. H. Solis, S. Hammes-Schiffer, *Inorg. Chem.*, 2014, **53**, 6427-6443. (e) A. Bhattacharjee, E. S. Andreiadis, M. Chavarot-Kerlidou, M. Fontecave, M. J. Field, V. Artero, *Chem. Eur. J.*, 2013, **19**, 15166-15174. (f) S. Kaur-Ghumaan, L. Schwartz, R. Lomoth, M. Stein, S. Ott, *Angew. Chem. Int. Ed*, 2010, **49**, 8033-8036. (g) D. J. Graham, D. G. Nocera, *Organometallics*, 2014, **33**, 4994-5001.
10 R. H. Crabtree, P. E. M. Siegbahn, O. Eisenstein, A. L. Rheingold, T. F. Koetzle, *Acc. Chem. Res.*, 1996, **29**, 348-354.
11 C. Gonzalez, H. B. Schlegel, *J. Chem. Phys.*, 1989, **90**, 2154-2161.
12 P. E. M. Siegbahn, J. W. Tye, M. B. Hall, *Chem. Rev.,* 2007, **107**, 4414-4435.
13 (a) Y. Wang, M. Wang, L. Sun, M. S. G. Ahlquist, *Chem. Commun.*, 2012, **48**, 4450-4452. (b) Y. Wang, M. S. G. Ahlquist, *Dalton Trans.,* 2013, **42**, 7816-7822.



 

Graphical abstract for:

# Mechanism of Hydrogen Evolution in Cu(bztpen)-Catalysed Water Reduction: A DFT Study

Rong-Zhen Liao, Mei Wang, Licheng Sun, and Per E. M. Siegbahn

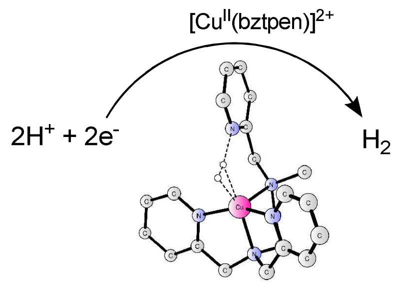


DFT calculations suggest hydrogen evolution proceeds via coupling of a Cu(II)-hydride and a pendant pyridinium.